

Anomalous metallic oxygen band in the potential superconductor $\text{KCa}_2\text{Fe}_4\text{As}_4\text{O}_2$

Nikita S. Pavlov^{a,b}, Kirill. S. Pervakov^b, Igor A. Nekrasov^{a,b}

^a*Institute for Electrophysics, Russian Academy of Sciences, Ekaterinburg, 620016, Russia*

^b*P. N. Lebedev Physical Institute, Russian Academy of Sciences, Moscow, 119991, Russia*

Abstract

The electronic structure, magnetism and Fermi surface of a hole self-doped potential iron-based superconductor $\text{KCa}_2\text{Fe}_4\text{As}_4\text{O}_2$ (12442) were studied by a first-principles DFT/GGA approach. The projection onto Wannier functions basis is proposed to calculate directly the self-doping value. In particular for $\text{KCa}_2\text{Fe}_4\text{As}_4\text{O}_2$ it is 0.75 hole on Fe-3d states. Surprisingly, for the $\text{KCa}_2\text{Fe}_4\text{As}_4\text{O}_2$ it was found that except the Fe-3d bands the O-2p bands also cross the Fermi level, which is quite anomalous behavior for O-2p states. In general, the O-2p states are usually fully occupied in transition metal oxides. Here it is not the case due to the fact that CaO layer gives some of the electrons to the FeAs layer, thus leaving O-2p states partially occupied. The O-2p states form additional Fermi surface sheet with propeller-like shape around Γ -point and modify the Fe-3d Fermi surface sheets due to the hybridization. To prove the presence of anomalous metallic O-2p band in $\text{KCa}_2\text{Fe}_4\text{As}_4\text{O}_2$ the comparative study with the same family systems $\text{KCa}_2\text{Fe}_4\text{As}_4\text{F}_2$ and $\text{RbGd}_2\text{Fe}_4\text{As}_4\text{O}_2$ (where it is not the case) was performed. The magnetic ground state is found to be antiferromagnetic with checkerboard ordering. Therefore, we expect that the $\text{KCa}_2\text{Fe}_4\text{As}_4\text{O}_2$ might be a potential superconductor with unusual properties.

Keywords: Iron-based superconductors, Electronic structure, self-doped superconductor, DFT/GGA

*Corresponding author

URL: pavlovns@lebedev.ru (Nikita S. Pavlov)

1. Introduction

The first discovery of superconductivity in 1144 ($\text{KCa}_2\text{Fe}_4\text{As}_4$ [1, 2]) and 12442 fluorine systems ($\text{KCa}_2\text{Fe}_4\text{As}_4\text{F}_2$ [3]) was made in 2016. After that, in 2017, the 12442 oxygen system was synthesized. Experimentally superconductivity was observed in $\text{RbGd}_2\text{Fe}_4\text{As}_4\text{O}_2$ ($T_c = 35$ K) [4], in $\text{BaTh}_2\text{Fe}_4\text{As}_4(\text{N}_{0.7}\text{O}_{0.3})_2$ ($T_c = 30$ K) [5] and in $\text{RbLn}_2\text{Fe}_4\text{As}_4\text{O}_2$ ($Ln = \text{Sm, Tb, Dy and Ho}$) ($T_c = 34 - 36$ K) [6]. A whole range of compounds with oxygen $ALn_2\text{Fe}_4\text{As}_4\text{O}_2$ ($A = \text{K and Cs}$; $Ln = \text{lanthanides}$) was experimentally investigated in the work [7] ($T_c = 33 - 37$ K).

To our knowledge, there is just one single DFT study of 12442 oxygen system – $\text{RbGd}_2\text{Fe}_4\text{As}_4\text{O}_2$ [8] and several DFT calculations of 12442 fluorine systems: $\text{KCa}_2\text{Fe}_4\text{As}_4\text{F}_2$ system [9, 10], $\text{KCa}_2\text{Fe}_4\text{As}_4\text{F}_2$ film [11] and $\text{CsCa}_2\text{Fe}_4\text{As}_4\text{F}_2$ [12]. Whereas several dozen of experimental papers are devoted to the 12442 fluorine compounds. Let us list below those works that we are aware of. The most studied system among them is $\text{KCa}_2\text{Fe}_4\text{As}_4\text{F}_2$ ($T_c = 33.36$ K) [13]. Fermi surface, quasiparticle bands and superconducting gap are investigated by ARPES for the system in [14]. A resistance and elastoresistance measurements were performed [15]. The critical current densities J_c through the $\text{KCa}_2\text{Fe}_4\text{As}_4\text{F}_2$ wire at 4.2 K is 10 kA/cm^2 under self-field, and 1 kA/cm^2 at 100 kOe [16]. Magnetic susceptibility and penetration depth are reported in [13]. The anisotropy parameter γ and London penetration depth λ were obtained from vortex torque [17]. An extremely high upper critical field ($H_{c2}(T) \sim 9$ T) for the fluorine compound was observed in [18]. Strong Pauli paramagnetic effect in the upper critical field was reported in [19]. An inelastic neutron scattering study on the low-energy spin excitations was done in the Ref. [20]. A systematic study of electrical resistivity, Hall coefficient, magneto-optical imaging, magnetization, and scanning transmission electron microscopy (STEM) analyses of single crystals was performed in the work [21]. Temperature-pressure phase diagram was investigated in [22]. Low-temperature specific heat (SH) is measured [23]. Nuclear magnetic resonance (NMR) study was done [24, 25].

The correlations between T_c and structural parameters was measured and discussed for $ACa_2Fe_4As_4F_2$ ($A = Rb, Cs$) compounds [26]. A transport and magnetic properties of the cobalt substitution in the intrinsically hole-doped $KCa_2(Fe_{1-x}Co_x)_4As_4F_2$ are investigated in [27]. A transport and magnetic measurements in single crystals of $CsCa_2Fe_4As_4F_2$ were performed in [28]. The thermal conductivity, resistivity, upper critical field $H_{c2}(T)$ of $CsCa_2Fe_4As_4F_2$ were investigated in [29]. The vortex phase diagram of $RbCa_2Fe_4As_4F_2$ via magneto-transport and magnetization measurements was performed in [30].

In this paper we investigate the electronic structure, magnetism and Fermi surface of a hole self-doped potential iron-based superconductor $KCa_2Fe_4As_4O_2$ within DFT/GGA approach. The Wannier functions analysis is proposed to obtain the self-doping value and the value was found to be 0.75 hole per Fe ion. Surprisingly, the O-2p band crosses the Fermi level and has a metallic behavior. The O-2p states occupancy per O ion is about 5.5 (instead of fully occupied value of 6) which is also obtained from Wannier functions analysis. To demonstrate the presence of anomalous metallic O-2p band in $KCa_2Fe_4As_4O_2$ the comparative study of its band structure with $KCa_2Fe_4As_4F_2$ and $RbGd_2Fe_4As_4O_2$ systems was performed.

2. Computational details

Since the $KCa_2Fe_4As_4O_2$ compound has not been synthesized yet, we use the space group and lattice parameters for $KCa_2Fe_4As_4F_2$ [3]. The crystal structure of $KCa_2Fe_4As_4F_2$ has the tetragonal symmetry with $I4/mmm$ space group at room temperature and the lattice constants $a = b = 3.8684 \text{ \AA}$ and $c = 31.007 \text{ \AA}$ [3]. The DFT calculations were performed within the full-potential linearized augmented plane-wave (FP-LAPW) code WIEN2k [31] with Perdew-Burke-Ernzerhof generalized gradient approximation of exchange correlation functional (GGA) [32]. The ion positions were DFT optimized for $KCa_2Fe_4As_4O_2$ starting with those for $KCa_2Fe_4As_4F_2$ (see Table 1). The Brillouin zone k-points grid was taken to be $16 \times 16 \times 16$.

Table 1: The optimized ion positions of paramagnetic $\text{KCa}_2\text{Fe}_4\text{As}_4\text{O}_2$. The ion positions of $\text{KCa}_2\text{Fe}_4\text{As}_4\text{F}_2$ from [3] are shown in brackets. dFe-As1 and As1-Fe-As1 angle

atom	site	x	y	z
K	2a	0	0	0
Ca	4e	0.5	0.5	0.21583 (0.2085)
Fe	8g	0	0.5	0.10784 (0.1108)
As1	4e	0.5	0.5	0.06604 (0.0655)
As2	4e	0	0	0.14880 (0.1571)
O (F)	4d	0	0.5	0.25

For DFT calculation of $\text{KCa}_2\text{Fe}_4\text{As}_4\text{F}_2$ the experimental ion positions were used [3] which are shown in brackets in Table 1. The Quantum Espresso [33] was used for calculation of $\text{RbGd}_2\text{Fe}_4\text{As}_4\text{O}_2$ with the Gd-4f states considered as a part of the core states. The projected augmented wave pseudopotentials (PAW) were applied. The ion positions of $\text{RbGd}_2\text{Fe}_4\text{As}_4\text{O}_2$ were taken from [8].

To calculate shell and orbital occupancies the DFT/GGA Hamiltonian was projected onto Fe-3d, As-4p (O-2p) Wannier functions. The obtained Wannier-projected dispersions perfectly coincide with the DFT ones. Wannier functions are obtained within Wannier90 code [34].

3. Results and discussion

The GGA densities of states (total and partial) and band dispersions of paramagnetic $\text{KCa}_2\text{Fe}_4\text{As}_4\text{O}_2$ are shown in Fig. 1. As usual for the iron-based superconductors the main contribution to the density of states at the Fermi level comes from Fe-3d states. But in this compound surprisingly the O-2p states (which are located from -2.8 eV to 0.12 eV) appear at the Fermi level as well. It is quite unusual, anomalous behavior, because typically the O-2p states are fully occupied and lie in the energy interval from -6 eV to -2 eV. It means that in $\text{KCa}_2\text{Fe}_4\text{As}_4\text{O}_2$ system the O-2p states of CaO layer do not receive enough electrons to get filled completely. Thus the CaO layer gives some

of the electrons to the FeAs layer. The O-2p states at the Fermi level are mostly hybridized with the Fe-3d_{xy} orbital.

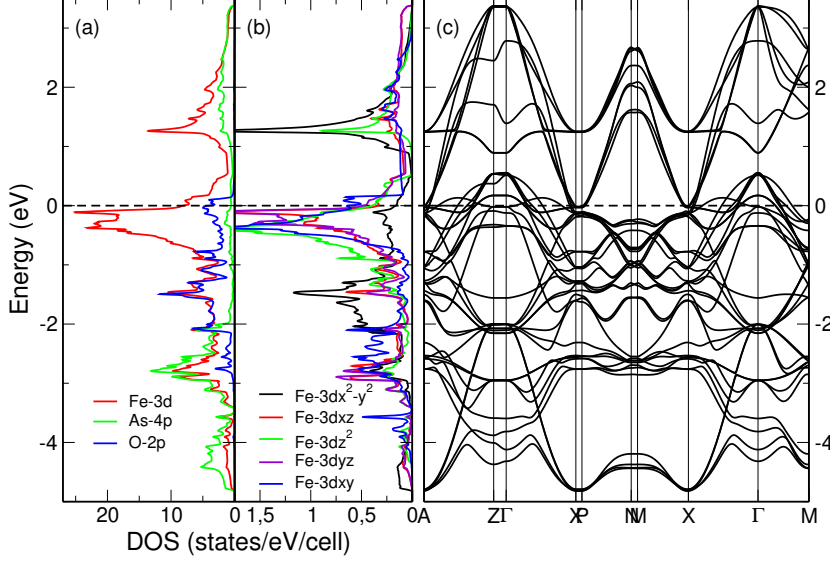


Figure 1: DFT/GGA (a) densities of states (Fe-3d, As-4p, O-2p), (b) densities of Fe-3d states and (c) band dispersions of paramagnetic $\text{KCa}_2\text{Fe}_4\text{As}_4\text{O}_2$. The Fermi level is at zero energy.

There is the sharp peak of Fe-3d_{xz} and Fe-3d_{yz} states just below the Fermi level, which may be important for superconductivity in case of the hole doping. The Fe-3d_{xz} and Fe-3d_{yz} bands become non-degenerate because of the different z_{As} distances below and above Fe ion plane since As has different neighbors there Ca or K. The contribution to the density of states of Fe-3d(xz, yz, z^2) orbitals is nearly the same at the Fermi level, while the contribution of Fe-3d_{xy} is two times larger than later ones and Fe-3d_{x²-y²} – three times smaller. The As-4p states are located in interval from -4.8 eV to -2 eV.

We compare the densities of states for $\text{KCa}_2\text{Fe}_4\text{As}_4\text{O}_2$ with ones of the $\text{RbGd}_2\text{Fe}_4\text{As}_4\text{O}_2$ to show the difference of the O-2p states energy position between them (see Fig. 2). For completeness the densities of states of fluorine $\text{KCa}_2\text{Fe}_4\text{As}_4\text{F}_2$ system is also presented on Fig. 2. In $\text{KCa}_2\text{Fe}_4\text{As}_4\text{F}_2$ and $\text{RbGd}_2\text{Fe}_4\text{As}_4\text{O}_2$ systems the F-2p and O-2p states are fully occupied and are

located well below the Fermi level. The Fe-3d and As-4p states are similar to each other in shape and energy position for all three systems. It should be noted that among all considered systems the $\text{KCa}_2\text{Fe}_4\text{As}_4\text{O}_2$ system has the largest value of density of states at the Fermi level. Although the Fe-3d density of states at the Fermi level is equal to those of $\text{KCa}_2\text{Fe}_4\text{As}_4\text{O}_2$ and $\text{KCa}_2\text{Fe}_4\text{As}_4\text{F}_2$, the difference comes due to the O-2p states presence at the Fermi level.

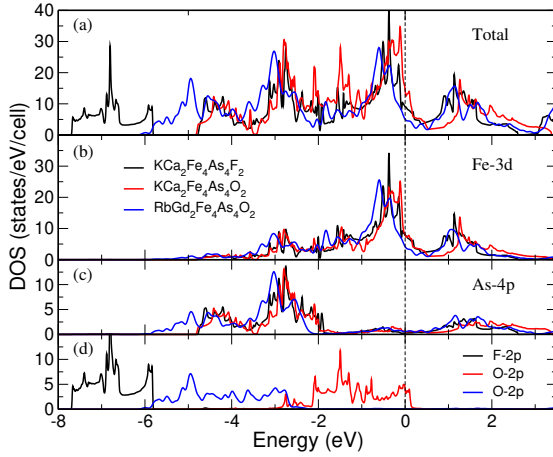


Figure 2: Comparison of DFT/GGA densities of states of $\text{KCa}_2\text{Fe}_4\text{As}_4\text{O}_2$ (red lines), $\text{KCa}_2\text{Fe}_4\text{As}_4\text{F}_2$ (black lines) and $\text{RbGd}_2\text{Fe}_4\text{As}_4\text{O}_2$ (blue lines): (a) total, (b) Fe-3d states, (c) As-4p states, (d) O-2p (F-2p) states.

Let's compare the band dispersions of $\text{KCa}_2\text{Fe}_4\text{As}_4\text{O}_2$ (red lines) and $\text{KCa}_2\text{Fe}_4\text{As}_4\text{F}_2$ (black lines) near the Fermi level on Fig. 3. In general, $\text{KCa}_2\text{Fe}_4\text{As}_4\text{F}_2$ bands (black lines) are about 0.1-0.2 eV lower in energy than $\text{KCa}_2\text{Fe}_4\text{As}_4\text{O}_2$ bands (red lines) since the fluorine system has two more electrons than the oxygen one. Whereas, some bands have similar positions. However, in $\text{KCa}_2\text{Fe}_4\text{As}_4\text{O}_2$ system there is additional band in the middle of Γ -X (A-Z) direction, which crosses the Fermi level. This band is formed by the O-2p_x and O-2p_y orbitals as can be seen on Fig. 4(g).

Quite important question is how to calculate the self-doping value in the $\text{KCa}_2\text{Fe}_4\text{As}_4\text{O}_2$ system. In general, in the parent iron-based compounds (for example, NaFeAs, BaFe₂As₂, LaOFeAs) valance of Fe is 2+ which corresponds

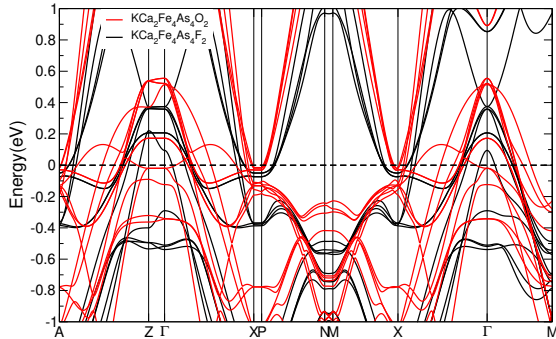


Figure 3: Comparison of DFT/GGA band dispersions of paramagnetic $\text{KCa}_2\text{Fe}_4\text{As}_4\text{O}_2$ (red lines) with $\text{KCa}_2\text{Fe}_4\text{As}_4\text{F}_2$ system (black lines), which has two more electrons per formula unit.

to 6 electrons on Fe-3d shell and empty Fe-4s shell. The self-doping means that for the stoichiometric system Fe-3d has less or more than 6 electrons and the valence of Fe is different from 2+. One can calculate the formal valence of Fe in $\text{KCa}_2\text{Fe}_4\text{As}_4\text{O}_2$ by assuming the valencies of K^+ , Ca^{2+} , As^{3-} and O^{2-} are known. As the result the valence of Fe will be 2.75+ (0.75 hole/Fe-3d).

The simplest way to estimate the self-doping value from DFT is just to take the values of DFT occupancies for instance in this work they are 6.12 for Fe-3d and 2.92 for As-4p. But the As-4p states are located below the Fermi level (Fig. 1), therefore, they are fully occupied and must have 6 electrons. The reason of the discrepancy in DFT As-4p occupancy is that the DOS of As-4p states is spread in energy due to the hybridization with other states including strong hybridization with Fe-3d states. In DFT, the total number of electrons is strictly fixed, but it can be difficult to calculate the partial contributions due to the hybridization. To overcome this circumstance, we propose to use Wannier function projection, since Wannier functions are maximally localized and have atomic-like nature. It allows one to exclude the “parasitic” hybridization.

If it could be possible to disentangle the Fe-3d and As-4p bands and project only onto Fe-3d states, then one could immediately obtain a filling of the Fe-3d shell. In case of $\text{KCa}_2\text{Fe}_4\text{As}_4\text{O}_2$, this cannot be done with satisfactory agreement

between DFT and Wannier function projected bands. Therefore, we chose the Wannier function basis consisting of Fe-3d and As-4p orbitals (4 Fe atoms and 4 As atoms) and obtain the total occupancy 44.96 (≈ 45). In general, the Fe-3d and As-4p states together have 12 electrons (6 electrons on Fe-3d and 6 electrons on As-4p), consequently the Fe_4As_4 block must have 48 electrons. It means in $\text{KCa}_2\text{Fe}_4\text{As}_4\text{O}_2$ there are 3 electrons less per Fe_4As_4 block. Assuming that the As-4p is filled completely the Fe-3d states must 5.25 electrons instead of 6. This occupancy is very close to half-filling. Thus, one can expect that Fe-3d electron-electron correlations might be noticeable. From Fe-3d filling one can calculate the valance of Fe, assuming that the Fe-4s states are fully empty. Hence the total number of holes on Fe can be found from sum $0.75 + 2.0 = 2.75$.

As mentioned above in $\text{KCa}_2\text{Fe}_4\text{As}_4\text{O}_2$ the O-2p states cross the Fermi level and thus are not fully occupied. We include the O-2p orbitals into Wannier function basis set and obtain the total occupancy of 55.96 (≈ 56) for 4 Fe atoms, 4 As atoms and 2 O atoms. Without self-doping this occupancy should be 60 ($4 * 6$ electrons on Fe-3d, $4 * 6$ electrons on As-4p and $2 * 6$ electrons on O-2p). Considering the result of projection to Fe-3d and As-4p orbitals, which have 3 electrons less, the O-2p states have 1 hole per 2 O atoms or 0.5 hole/O.

Let us perform the same analysis for $\text{KCa}_2\text{Fe}_4\text{As}_4\text{F}_2$ compound. In case of Wannier function basis is set to Fe-3d, As-4p (F-2p) orbitals the total occupancy after the projection is 46.39 (58.36). The F-2p states add another 12 electrons. Therefore, the F-2p state are fully occupied and have 6 electrons. While, the Fe_4As_4 block has 1.6 electrons less (0.4 hole/Fe-3d). The formal valence of Fe in $\text{KCa}_2\text{Fe}_4\text{As}_4\text{F}_2$ with F^- valence will be $2.25 + (0.25 \text{ hole/Fe-3d})$. For the $\text{KCa}_2\text{Fe}_4\text{As}_4\text{F}_2$ the Wannier function projection and formal valence calculation provide different values. It turns out that Fe get less electrons than expected from formal electroneutrality.

The projected bands of paramagnetic $\text{KCa}_2\text{Fe}_4\text{As}_4\text{O}_2$ onto the (a) Fe-3d (red lines) and O-2p (blue lines), (b) $\text{Fe-3d}_{x^2-y^2}$, (c) Fe-3d_{z^2} , (d) Fe-3d_{xy} , (e) Fe-3d_{xz} , (f) Fe-3d_{yz} , (g) $\text{O-2p}_x+2\text{p}_y$, (h) O-2p_z states are presented in Fig. 4. As can be seen from the density of states (Fig. 1), the contribution of $\text{Fe-3d}_{x^2-y^2}$

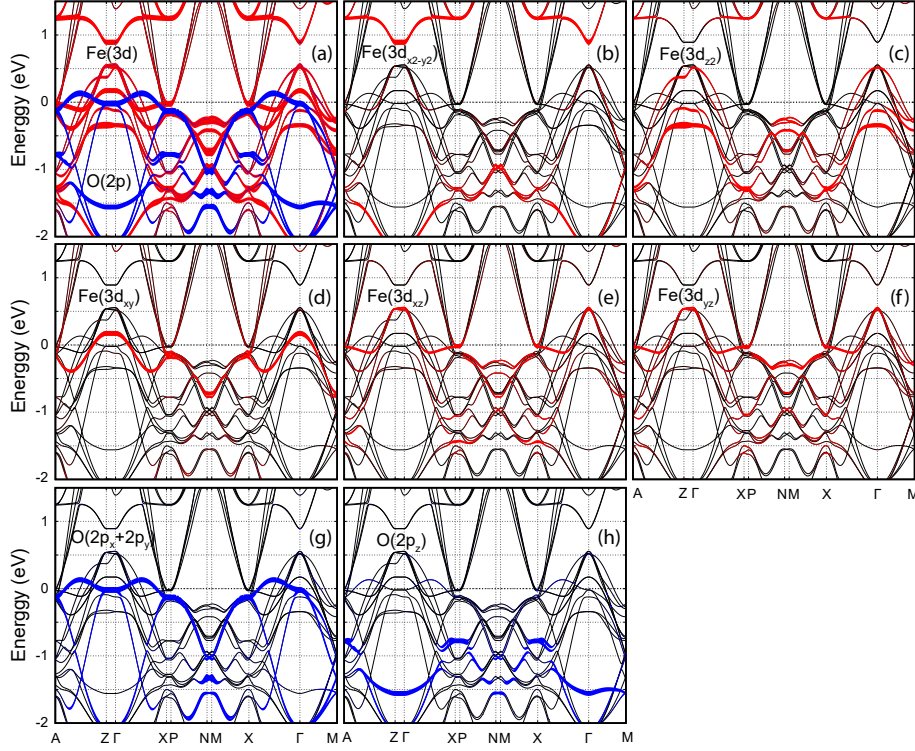


Figure 4: The projected band structure of paramagnetic $\text{KCa}_2\text{Fe}_4\text{As}_4\text{O}_2$, where the linewidth corresponds to the projected weight of Bloch states onto the (a) Fe-3d (red lines) and O-2p (blue lines), (b) Fe- $3d_{x^2-y^2}$, (c) Fe- $3d_{z^2}$, (d) Fe- $3d_{xy}$, (e) Fe- $3d_{xz}$, (f) Fe- $3d_{yz}$, (g) O- $2p_x+2p_y$, (h) O- $2p_z$ states.

orbital is quite far away from the Fermi level. All other Fe-3d orbitals are located in the vicinity of the Fermi level. The O- $2p_x+2p_y$ bands cross the Fermi level and are located between -2.8 and 0.12 eV.

In the LDA+DMFT investigation of 1144 system $\text{KCaFe}_4\text{As}_4$ [35] it was shown that the spin-orbit (SO) coupling is important due to glide-mirror symmetry breaking. We compare the band dispersion with and without SO near the Fermi level in Fig. 5. The SO gives rather small bands shift ~ 0.01 eV and bands splitting in A-Z, Γ -X directions around -0.11 eV. Thus one can note, that the SO almost does not affect on the band structure of $\text{KCa}_2\text{Fe}_4\text{As}_4\text{O}_2$.

In Fig. 6 the DFT calculated Fermi surface for $\text{KCa}_2\text{Fe}_4\text{As}_4\text{O}_2$ system is

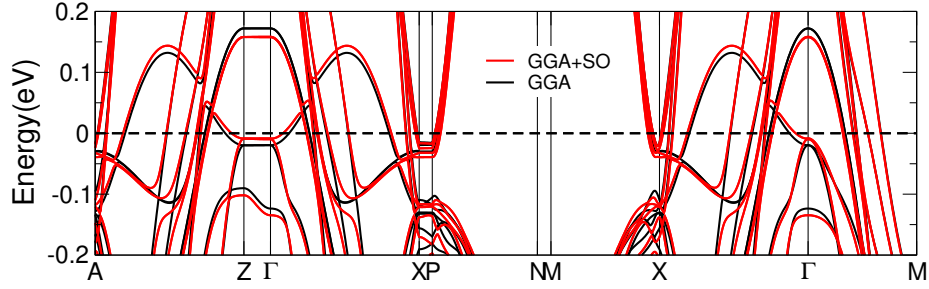


Figure 5: DFT/GGA band dispersions of paramagnetic $\text{KCa}_2\text{Fe}_4\text{As}_4\text{O}_2$ with spin-orbit coupling (SO) (red lines) and without SO (black lines).

presented. The Fermi surface sheet (Fig. 6a) with propeller shape around Γ -point corresponds to O-2p states. Due to hybridization the typically cylindrical in iron-based superconductors Fe-3d Fermi surface sheets here are modified.

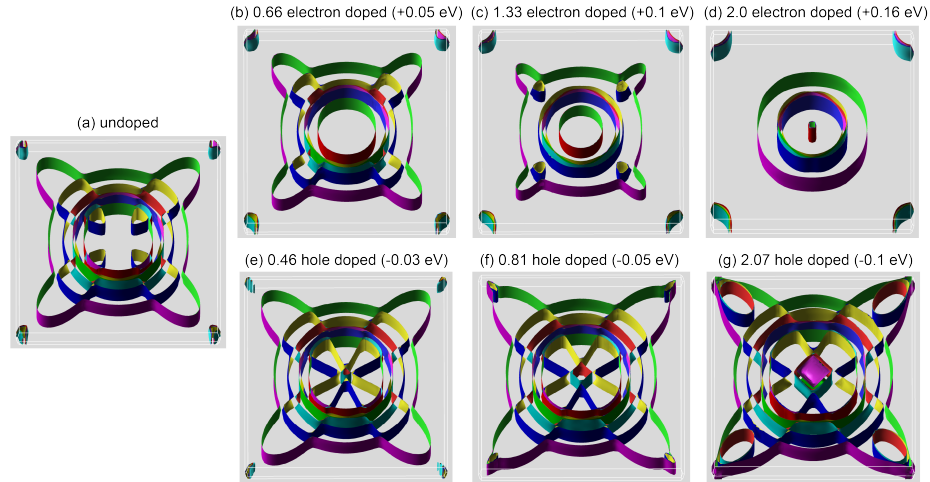


Figure 6: The Fermi surface of paramagnetic $\text{KCa}_2\text{Fe}_4\text{As}_4\text{O}_2$: (a) undoped case, (b) 0.66 electron doped (+0.05 eV rigid shift of Fermi level), (c) 1.33 electron doped (+0.1 eV shift), (d) 2.0 electron doped (+0.166 eV shift), (e) 0.46 hole doped (-0.03 eV shift), (f) 0.81 hole doped (-0.05 eV shift), (g) 2.07 hole doped (-0.1 eV shift).

Also the Fermi surfaces at different values of electron (b-d) and hole (e-g) doping levels introduced by a rigid band shift are shown in Fig. 6. The doping values correspond to Lifshitz transition or in other words appearance or disap-

pearance of some Fermi surface sheets. At electron doping level of 2.0 electrons per formula unit the O-2p Fermi surface sheet disappears, thus the Fermi surface of $\text{KCa}_2\text{Fe}_4\text{As}_4\text{O}_2$ system becomes similar to one of $\text{RbGd}_2\text{Fe}_4\text{As}_4\text{O}_2$ [8] or $\text{KCa}_2\text{Fe}_4\text{As}_4\text{F}_2$ system. For completeness, all 12 Fermi surface sheets are presented separately in Fig. 7 for stoichiometric $\text{KCa}_2\text{Fe}_4\text{As}_4\text{O}_2$.

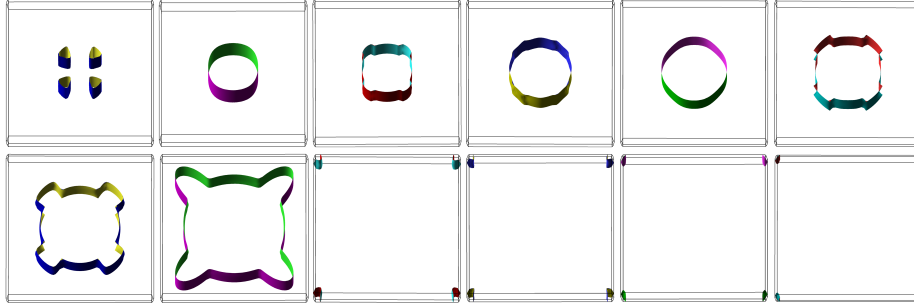


Figure 7: The Fermi surface of $\text{KCa}_2\text{Fe}_4\text{As}_4\text{O}_2$, each band is show separately.

And finally, we established the magnetic ground-state by calculating the total energy of different magnetic phases (see Table 2): paramagnetic phase (PM), ferromagnetic phase (FM), checkerboard antiferromagnetic phase (AFM1) (nearest-neighbor Fe spins antiparallel each other) and stripe antiferromagnetic phase (AFM2) (Fe spin moments parallel along one line of atoms and anti-parallel along neighbor line of atoms). The magnetic ground state of $\text{KCa}_2\text{Fe}_4\text{As}_4\text{O}_2$ is found to be checkerboard antiferromagnetic (AFM1) one with -41.1 meV per Fe atom lower than the PM state.

4. Conclusions

In this paper we performed the DFT/GGA first-principle calculations of hole self-doped potential iron-based superconductor $\text{KCa}_2\text{Fe}_4\text{As}_4\text{O}_2$. Most interesting result of our paper is presence at the Fermi level of anomalous metallic O-2p band which is formed by O-2p_x and O-2p_y orbitals. The Fermi surface sheet corresponding of O-ps states has propeller shape and has its center at Γ -point. The O-2p states are not filled completely. This tells us that the CaO layer gives

Table 2: The calculated total energy per Fe atom with respect to the paramagnetic phase (PM) and Fe magnetic moment of magnetic phases (AFM1 (Ch.B.) – checkerboard antiferromagnetic order, AFM2 – stripe antiferromagnetic order).

Order	Energy per Fe (meV)	Fe Magnetic Moment (μ_B)
PM	0	0
AFM2 (stripe)	-20.3	1.04
FM	-27.6	0.78
AFM1 (Ch.B.)	-41.1	1.64

some of the electrons to the FeAs layer. The cylindrical Fe-3d Fermi surface sheets are modified due to hybridization with O-2p Fermi surface sheet. Analysis of DOS obtained by the Wannier function projection provides self-doping value of Fe-As layer – 0.75 hole/Fe-3d. The similar analysis gives at O-2p states 5.5 electrons per O ion. The magnetic ground state is the checkerboard antiferromagnetic state. Also the comparative study of $\text{KCa}_2\text{Fe}_4\text{As}_4\text{O}_2$ with the same family systems $\text{KCa}_2\text{Fe}_4\text{As}_4\text{F}_2$ and $\text{RbGd}_2\text{Fe}_4\text{As}_4\text{O}_2$ was performed to prove that the $\text{KCa}_2\text{Fe}_4\text{As}_4\text{O}_2$ system is quite outstanding in this line. We believe that $\text{KCa}_2\text{Fe}_4\text{As}_4\text{O}_2$ might be a potential superconductor with possible unusual properties because of anomalous metallic O-2p band.

Acknowledgements

This work was supported in part by RSCF grant No. 21-12-00394.

References

- [1] A. Iyo, K. Kawashima, T. Kinjo, T. Nishio, S. Ishida, H. Fujihisa, Y. Gotoh, K. Kihou, H. Eisaki, Y. Yoshida, New-Structure-Type Fe-Based Superconductors: $\text{CaAFe}_4\text{As}_4$ ($A = \text{K, Rb, Cs}$) and $\text{SrAFe}_4\text{As}_4$ ($A = \text{Rb, Cs}$), *Journal of the American Chemical Society* 138 (10) (2016) 3410–3415. doi:10.1021/jacs.5b12571.
 URL <https://pubs.acs.org/doi/10.1021/jacs.5b12571>

- [2] D. Mou, T. Kong, W. R. Meier, F. Lochner, L.-L. Wang, Q. Lin, Y. Wu, S. L. Bud'ko, I. Eremin, D. D. Johnson, P. C. Canfield, A. Kaminski, Enhancement of the Superconducting Gap by Nesting in $\text{CaKFe}_4\text{As}_4$: A New High Temperature Superconductor, *Physical Review Letters* 117 (27) (2016) 277001. doi:10.1103/PhysRevLett.117.277001.
URL <https://link.aps.org/doi/10.1103/PhysRevLett.117.277001>
- [3] Z. C. Wang, C. Y. He, S. Q. Wu, Z. T. Tang, Y. Liu, A. Ablimit, C. M. Feng, G. H. Cao, Superconductivity in $\text{KCa}_2\text{Fe}_4\text{As}_4\text{F}_2$ with separate double Fe_2As_2 layers, *Journal of the American Chemical Society* 138 (25) (2016) 7856–7859. doi:10.1021/jacs.6b04538.
- [4] Z.-C. Wang, C.-Y. He, S.-Q. Wu, Z.-T. Tang, Y. Liu, A. Ablimit, Q. Tao, C.-M. Feng, Z.-A. Xu, G.-H. Cao, Superconductivity at 35 K by self doping in $\text{RbGd}_2\text{Fe}_4\text{As}_4\text{O}_2$, *Journal of Physics: Condensed Matter* 29 (11) (2017) 11LT01. doi:10.1088/1361-648X/aa58d2.
URL <https://iopscience.iop.org/article/10.1088/1361-648X/aa58d2>
- [5] Y.-t. Shao, Z.-c. Wang, B.-z. Li, S.-Q. Wu, J.-f. Wu, Z. Ren, S.-w. Qiu, C. Rao, C. Wang, G.-H. Cao, $\text{BaTh}_2\text{Fe}_4\text{As}_4(\text{N}_{0.7}\text{O}_{0.3})_2$: An iron-based superconductor stabilized by inter-block-layer charge transfer, *Science China Materials* 62 (9) (2019) 1357–1362. doi:10.1007/s40843-019-9438-7.
URL <http://link.springer.com/10.1007/s40843-019-9438-7>
- [6] Z. C. Wang, C. Y. He, S. Q. Wu, Z. T. Tang, Y. Liu, G. H. Cao, Synthesis, Crystal Structure and Superconductivity in $\text{RbLn}_2\text{Fe}_4\text{As}_4\text{O}_2$ ($\text{Ln} = \text{Sm}$, Tb , Dy and Ho), *Chemistry of Materials* 29 (4) (2017) 1805–1812. doi:10.1021/acs.chemmater.6b05458.
- [7] S.-Q. Wu, Z.-C. Wang, C.-Y. He, Z.-T. Tang, Y. Liu, G.-H. Cao, Superconductivity at 33-37 K in $\text{ALn}_2\text{Fe}_4\text{As}_4\text{O}_2$ ($A = \text{K}$ and Cs ; $\text{Ln} = \text{lanthanides}$), *Physical Review Materials* 1 (4) (2017) 044804. doi:10.1103/PhysRevMaterials.1.044804.

URL <https://link.aps.org/doi/10.1103/PhysRevMaterials.1.044804>

- [8] Z. Wang, G. Wang, X. Tian, Electronic structure and magnetism of $\text{RbGd}_2\text{Fe}_4\text{As}_4\text{O}_{12}$, *Journal of Alloys and Compounds* 708 (2017) 392–396. doi:10.1016/j.jallcom.2017.03.017.
URL <http://dx.doi.org/10.1016/j.jallcom.2017.03.017>
- [9] G. Wang, Z. Wang, X. Shi, Self-hole-doping-induced superconductivity in $\text{KCa}_2\text{Fe}_4\text{As}_4\text{F}_2$, *EPL (Europhysics Letters)* 116 (3) (2016) 37003. doi:10.1209/0295-5075/116/37003.
URL <http://link.springer.com/10.1007/s10948-019-05367-3https://iopscience.iop.org/article/10.1209/0295-5075/116/37003>
- [10] Density functional study of $\text{ACa}_2\text{Fe}_4\text{As}_4\text{F}_2$ ($A = \text{K}, \text{Rb}$): Electronic structure, unconventional superconductors, in: *AIP Conference Proceedings*, Vol. 2009, 2018, p. 020002. doi:10.1063/1.5052071.
URL <http://aip.scitation.org/doi/abs/10.1063/1.5052071>
- [11] X. Li, C. Huang, Y. Zhu, Y. Zhang, Magnetic Orders and Electronic Structures of Compressive- and Tensile-Strained $\text{KCa}_2\text{Fe}_4\text{As}_4\text{F}_2$ Films, *Journal of Superconductivity and Novel Magnetism* 33 (5) (2020) 1377–1383. doi:10.1007/s10948-019-05367-3.
- [12] B. Singh, P. Kumar, Unconventional iron-based superconductor $\text{CsCa}_2\text{Fe}_4\text{As}_4\text{F}_2$: A first-principle study, in: *AIP Conference Proceedings*, Vol. 1953, 2019, p. 120019. doi:10.1063/1.5033084.
URL <http://aip.scitation.org/doi/abs/10.1063/1.5033084>
- [13] M. Smidman, F. K. K. Kirschner, D. T. Adroja, A. D. Hillier, F. Lang, Z. C. Wang, G. H. Cao, S. J. Blundell, Nodal multigap superconductivity in $\text{KCa}_2\text{Fe}_4\text{As}_4\text{F}_2$, *Physical Review B* 97 (6) (2018) 060509. doi:10.1103/PhysRevB.97.060509.
URL <https://link.aps.org/doi/10.1103/PhysRevB.97.060509>

- [14] D. Wu, W. Hong, C. Dong, X. Wu, Q. Sui, J. Huang, Q. Gao, C. Li, C. Song, H. Luo, C. Yin, Y. Xu, X. Luo, Y. Cai, J. Jia, Q. Wang, Y. Huang, G. Liu, S. Zhang, F. Zhang, F. Yang, Z. Wang, Q. Peng, Z. Xu, X. Qiu, S. Li, H. Luo, J. Hu, L. Zhao, X. J. Zhou, Spectroscopic evidence of bilayer splitting and strong interlayer pairing in the superconductor $\text{KCa}_2\text{Fe}_4\text{As}_4\text{F}_2$ Dingsong, *Physical Review B* 101 (22) (2020) 224508. doi:10.1103/PhysRevB.101.224508.
URL <https://link.aps.org/doi/10.1103/PhysRevB.101.224508>
- [15] T. Terashima, Y. Matsushita, H. Yamase, N. Kikugawa, H. Abe, M. Imai, S. Uji, S. Ishida, H. Eisaki, A. Iyo, K. Kihou, C.-H. Lee, T. Wang, G. Mu, Elastoresistance measurements on $\text{CaKFe}_4\text{As}_4$ and $\text{KCa}_2\text{Fe}_4\text{As}_4\text{F}_2$ with the Fe site of C_{2v} symmetry, *Physical Review B* 102 (5) (2020) 054511. doi:10.1103/PhysRevB.102.054511.
URL <https://link.aps.org/doi/10.1103/PhysRevB.102.054511>
- [16]
- [17] A. B. Yu, T. Wang, Y. F. Wu, Z. Huang, H. Xiao, G. Mu, T. Hu, Probing superconducting anisotropy of single crystal $\text{KCa}_2\text{Fe}_4\text{As}_4\text{F}_2$ by magnetic torque measurements, *Physical Review B* 100 (14) (2019) 144505. doi:10.1103/PhysRevB.100.144505.
URL <https://link.aps.org/doi/10.1103/PhysRevB.100.144505>
- [18] T. Wang, J. Chu, H. Jin, J. Feng, L. Wang, Y. Song, C. Zhang, X. Xu, W. Li, Z. Li, T. Hu, D. Jiang, W. Peng, X. Liu, G. Mu, Single-Crystal Growth and Extremely High H_{c2} of 12442-Type Fe-Based Superconductor $\text{KCa}_2\text{Fe}_4\text{As}_4\text{F}_2$, *Journal of Physical Chemistry C* 123 (22) (2019) 13925–13929. doi:10.1021/acs.jpcc.9b04624.
- [19] T. Wang, C. Zhang, L. Xu, J. Wang, S. Jiang, Z. Zhu, Z. Wang, J. Chu, J. Feng, L. Wang, W. Li, T. Hu, X. Liu, G. Mu, Strong Pauli paramagnetic effect in the upper critical field of $\text{KCa}_2\text{Fe}_4\text{As}_4\text{F}_2$, *Science China Physics, Mechanics & Astronomy* 63 (2) (2020) 227412. doi:10.1007/

s11433-019-1441-4.

URL <http://link.springer.com/10.1007/s11433-019-1441-4>

- [20] W. Hong, L. Song, B. Liu, Z. Li, Z. Zeng, Y. Li, D. Wu, Q. Sui, T. Xie, S. Danilkin, H. Ghosh, A. Ghosh, J. Hu, L. Zhao, X. Zhou, X. Qiu, S. Li, H. Luo, Neutron Spin Resonance in a Quasi-Two-Dimensional Iron-Based Superconductor, *Physical Review Letters* 125 (11) (2020) 117002. doi: 10.1103/PHYSREVLETT.125.117002.
URL <https://doi.org/10.1103/PhysRevLett.125.117002>

- [21] S. Pyon, Y. Kobayashi, A. Takahashi, W. Li, T. Wang, G. Mu, A. Ichinose, T. Kambara, A. Yoshida, T. Tamegai, Anisotropic physical properties and large critical current density in $\text{KCa}_2\text{Fe}_4\text{As}_4\text{F}_2$ single crystal, *Physical Review Materials* 4 (10) (2020) 104801. doi:10.1103/PhysRevMaterials.4.104801.
URL <https://link.aps.org/doi/10.1103/PhysRevMaterials.4.104801>

- [22] B. Wang, Z.-C. Wang, K. Ishigaki, K. Matsubayashi, T. Eto, J. Sun, J.-G. Cheng, G.-H. Cao, Y. Uwatoko, Pressure-induced enhancement of superconductivity and quantum criticality in the 12442-type hybrid-structure superconductor $\text{KCa}_2\text{Fe}_4\text{As}_4\text{F}_2$, *Physical Review B* 99 (1) (2019) 014501. doi:10.1103/PhysRevB.99.014501.
URL <https://link.aps.org/doi/10.1103/PhysRevB.99.014501>

- [23] T. Wang, J. Chu, J. Feng, L. Wang, X. Xu, W. Li, H. Wen, X. Liu, G. Mu, Low temperature specific heat of 12442-type $\text{KCa}_2\text{Fe}_4\text{As}_4\text{F}_2$ single crystals, *Science China Physics, Mechanics & Astronomy* 63 (9) (2020) 297412. doi: 10.1007/s11433-020-1549-9.
URL <https://link.springer.com/10.1007/s11433-020-1549-9>

- [24] Z. C. Wang, C. Y. He, S. Q. Wu, Z. T. Tang, Y. Liu, G. H. Cao, Synthesis, Crystal Structure and Superconductivity in $\text{RbLn}_2\text{Fe}_4\text{As}_4\text{O}_2$ ($\text{Ln} = \text{Sm}$,

- Tb, Dy, and Ho), *Chemistry of Materials* 29 (4) (2017) 1805–1812. doi: 10.1021/acs.chemmater.6b05458.
- [25] J. Luo, C. Wang, Z. Wang, Q. Guo, J. Yang, R. Zhou, K. Matano, T. Oguchi, Z. Ren, G. Cao, G.-Q. Zheng, NMR and NQR studies on transition-metal arsenide superconductors LaRu₂As₂, KCa₂Fe₄As₄F₂, and A₂Cr₃As₃, *Chinese Physics B* 29 (6) (2020) 067402. doi:10.1088/1674-1056/ab892d.
URL <https://iopscience.iop.org/article/10.1088/2053-1583/abe778https://iopscience.iop.org/article/10.1088/1674-1056/ab892d>
- [26] Z. C. Wang, C. Y. He, S. Q. Wu, Z. T. Tang, Y. Liu, G. H. Cao, Synthesis, Crystal Structure and Superconductivity in RbLn₂Fe₄As₄O₂ (Ln = Sm, Tb, Dy, and Ho), *Chemistry of Materials* 29 (4) (2017) 1805–1812. doi: 10.1021/acs.chemmater.6b05458.
- [27] J. Ishida, S. Iimura, H. Hosono, Effects of disorder on the intrinsically hole-doped iron-based superconductor KCa₂Fe₄As₄F₂ by cobalt substitution, *Physical Review B* 96 (17) (2017) 174522. doi:10.1103/PhysRevB.96.174522.
URL <https://link.aps.org/doi/10.1103/PhysRevB.96.174522>
- [28] Z.-C. Wang, Y. Liu, S.-Q. Wu, Y.-T. Shao, Z. Ren, G.-H. Cao, Giant anisotropy in superconducting single crystals of CsCa₂Fe₄As₄F₂, *Physical Review B* 99 (14) (2019) 144501. doi:10.1103/PhysRevB.99.144501.
URL <https://link.aps.org/doi/10.1103/PhysRevB.99.144501>
- [29] Y. Y. Huang, Z. C. Wang, Y. J. Yu, J. M. Ni, Q. Li, E. J. Cheng, G. H. Cao, S. Y. Li, Multigap nodeless superconductivity in CsCa₂Fe₄As₄F₂ probed by heat transport, *Physical Review B* 99 (2) (2019) 020502. arXiv: 1811.06379, doi:10.1103/PhysRevB.99.020502.
URL <https://link.aps.org/doi/10.1103/PhysRevB.99.020502>

- [30] X. Xing, X. Yi, M. Li, Y. Meng, G. Mu, J.-Y. Ge, Z. Shi, Vortex phase diagram in 12442-type RbCa₂Fe₄As₄F₂ single crystal revealed by magnetotransport and magnetization measurements, *Superconductor Science and Technology* 33 (11) (2020) 114005. doi:10.1088/1361-6668/abb35f.
URL <https://doi.org/10.1088/1361-6668/abb35f>
- [31] P. Blaha, K. Schwarz, F. Tran, R. Laskowski, G. K. Madsen, L. D. Marks, WIEN2k: An APW+lo program for calculating the properties of solids, *The Journal of chemical physics* 152 (7) (2020) 074101. doi:10.1063/1.5143061.
URL <https://doi.org/10.1063/1.5143061>
- [32] J. P. Perdew, K. Burke, M. Ernzerhof, Generalized gradient approximation made simple, *Physical Review Letters* 77 (18) (1996) 3865–3868. doi:10.1103/PhysRevLett.77.3865.
- [33] QUANTUM ESPRESSO: a modular and open-source software project for quantum simulations of materials, *Journal of Physics: Condensed Matter* 21 (39) (2009) 395502. doi:10.1088/0953-8984/21/39/395502.
URL <https://iopscience.iop.org/article/10.1088/0953-8984/21/39/395502>
- [34] G. Pizzi, V. Vitale, R. Arita, S. Blügel, F. Freimuth, G. Géranton, M. Gibertini, D. Gresch, C. Johnson, T. Koretsune, J. Ibañez-Azpiroz, H. Lee, J.-M. Lihm, D. Marchand, A. Marrazzo, Y. Mokrousov, J. I. Mustafa, Y. No-hara, Y. Nomura, L. Paulatto, S. Poncé, T. Ponweiser, J. Qiao, F. Thöle, S. S. Tsirkin, M. Wierzbowska, N. Marzari, D. Vanderbilt, I. Souza, A. A. Mostofi, J. R. Yates, Wannier90 as a community code: new features and applications, *Journal of Physics: Condensed Matter* 32 (16) (2020) 165902. doi:10.1088/1361-648x/ab51ff.
- [35] W. Liu, L. Cao, S. Zhu, L. Kong, G. Wang, M. Papaj, P. Zhang, Y.-B. Liu, H. Chen, G. Li, F. Yang, T. Kondo, S. Du, G.-H. Cao, S. Shin,

L. Fu, Z. Yin, H.-J. Gao, H. Ding, A new Majorana platform in an Fe-As bilayer superconductor, *Nature Communications* 11 (1) (2020) 5688.
doi:10.1038/s41467-020-19487-1.
URL <http://www.nature.com/articles/s41467-020-19487-1>